Numerical Optimization and Wind-Tunnel Testing of Low Reynolds-Number Airfoils

Th. Lutz*, W. Würz* and S. Wagner†
University of Stuttgart, D-70550 Stuttgart, Germany

Abstract

A numerical optimization tool has been applied to the design of low Reynolds number airfoils ($200,000 \leqq Re \leqq 400,000$). The aerodynamic model is based on the Eppler code with major extensions. A new, robust model for the calculation of short transitional separation bubbles was implemented, along with an e^n transition criterion and Drela's turbulent boundary-layer procedure with a modified shape-factor relation. The method was coupled with a commercial hybrid optimizer and applied to perform unconstrained high degree of freedom optimizations with objective to minimize the drag for a specified lift range. One resulting airfoil was tested in the Model Wind-Tunnel (MWT) of the institute and compared to the classical RG-15 airfoil.

In order to allow a realistic recalculation of experiments conducted in the MWT the limiting n-factor was evaluated for this facility. A special airfoil featuring an extensive instability zone was designed for this purpose. The investigation was supplemented by detailed measurements of the turbulence level.

To get more insight in design guidelines for very low Reynolds number airfoils the influence of variations of the leading-edge geometry on the aerodynamic characteristics was studied experimentally at $Re = 50,000$.

1 Introduction

For the Reynolds-number regime of aircraft wing-sections ($Re \gtrapprox 1 \cdot 10^6$) sophisticated direct and inverse methods for airfoil analysis and design are available.[1,2] In the hands of experienced users these methods allow a carefully directed airfoil design. Usually, specific airfoils are being developed for any new aircraft in order to maximize the performance for the intended range of application.[2–6] Wind-tunnel tests mainly serve for verification of the predicted aerodynamic characteristics and are necessary means to determine the stall behavior and to optimize turbulators or the flap settings. Doubtless, the total number of design loops was significantly reduced due to the availability of reliable prediction methods.

This does not hold for the airfoil design at low Reynolds numbers ($Re \lessapprox 200,000$). In this regime, transition usually takes place in a separated boundary-layer if the clean airfoil is considered. To predict the influence of laminar separation, of (unsteady) transitional separation bubbles and of the viscous/inviscid interaction is still a challenge. This is especially true in the range of the critical Reynolds number where strong nonlinearities occur. In general, the uncertainty in the airfoil analysis increases with decreasing Re. For this reason it is necessary to include the lessons learned from wind-tunnel tests in the design methodology of low Reynolds number airfoils. Extensive experiments, physical interpretation of the results

*Research Assistant, Institute for Aerodynamics und Gas Dynamics (IAG), Pfaffenwaldring 21.

†Professor, Head of Institute, Institute for Aerodynamics und Gas Dynamics (IAG), Pfaffenwaldring 21.

and the transfer into successively improved airfoil designs, as performed e. g. by Selig et al.[7,8] is therefore the most promising approach.

Being aware of the above mentioned problems an attempt was made to perform direct numerical shape optimizations of low Reynolds number airfoils ($Re > 200,000$). This approach is considered to be instructive for two reasons: First, the optimizer may find unconventional solutions which could inspire new ideas for an improved manual design. Second, weak points of the aerodynamic model can be identified if the optimized airfoils are examined in a wind-tunnel test. This in turn may lead to improvements of the prediction methods.

The intention of the present optimizations was to perform an unconstrained design of completely new airfoils rather than to modify existing ones. This necessitates considering a large number of design variables in order to enable a detailed representation of the airfoil shape and the pressure distribution. Furthermore, stochastic optimization algorithms should be applied to reduce the possibility of getting trapped in a local optimum. A high degree of freedom problem in combination with a stochastic optimization strategy, however, requires a very large number of airfoils to be generated and analyzed until the optimization process converges. If the optimizations are to be performed with acceptable computation time a most efficient aerodynamic model is needed. For the present investigations a potential-flow method coupled with an integral boundary-layer procedure, a simplified bubble model and an e^n database-method for transition prediction was applied. Viscous/inviscid interaction was neglected in order to minimize the computational effort which actually is roughly two orders of magnitude below an XFOIL analysis. The complete airfoil optimization tool has been proven successful for the design of high Reynolds number ($Re \geqq 1 \cdot 10^6$) NLF airfoils[9,10] and is routinely applied for various design tasks.

In the following sections the ingredients of the method will briefly be described. Thereafter optimization examples of low Reynolds number airfoils including wind-tunnel verification will be discussed.

Supplementary to this theoretical approach to airfoil design fundamental wind-tunnel tests for very low Reynolds-number airfoils ($Re \lessapprox 50,000$) will be presented. First detailed experimental investigations of airfoil characteristics for this Reynolds-number regime were published by Schmitz.[11] He proved that thin airfoils featuring a sharp leading edge have a lower critical Reynolds number than 'conventional' airfoil designs. In the experiments of Schmitz the cambered plate (Gö 417a) shows the best performance up to $Re \approx 100,000$.

The problem of how to provoke boundary-layer transition for $Re < 50,000$ in order to avoid extensive laminar separation was examined by Hamma.[12] Among other designs a 9.7% thick symmetrical airfoil with a sharp leading edge was tested in a water tunnel and showed promising results. However, very complex flow phenomena were observed. For example, laminar separation with laminar reattachment, partly followed by a transitional separation bubble occurred for a specific α- and Re-regime. Furthermore, the separation angle abruptly increased for a distinct angle of attack. Such complex flow phenomena cannot be predicted reliably with available theoretical models. The present authors, therefore, prefer an experiment-based approach with the intention to establish guidelines for the design of very low Reynolds-number airfoils. In a recent test campaign the influence of relevant geometric parameters, like the leading-edge radius, on the aerodynamic performance has been examined. First results have been obtained and will be discussed.

2 Aerodynamic Model

For the present investigations the determination of the airfoil characteristics during the optimization process is based on the airfoil design and analysis method of Eppler.[2] Major extensions with respect to boundary-layer computation were added to this tool.

In the direct mode the inviscid outer-flow is evaluated by means of a higher-order panel method whereas an inverse conformal mapping procedure is used in the design mode. Based on the inviscid velocity distribution, the boundary-layer development is calculated with a first-order integral procedure.[2] The method is based on the numerical integration of von Kármán's integral momentum equation and Wieghardt's energy equation with the momentum thickness δ_2 and the energy thickness δ_3 as dependent variables. For attached laminar flow, algebraic closure relations are used which were derived from Falkner-Skan self-similar profiles in regions with adverse pressure gradient, whereas solutions for the flat plate with suction serve as a basis in accelerated flow regimes.

For the calculation of turbulent boundary-layers the method proposed by Drela[1] was implemented in the Eppler code with a new shape-factor relation $H_{12}\,(H_{32}, Re_{\delta_2})$. With this approach, Green's 'lag-equation' is introduced as a third governing equation in order to account for history effects in case of non-equilibrium flows. To close the problem Drela proposed an algebraic shape-factor relation which was derived from an evaluation of Swafford's two-parameter boundary-layer profiles. For very low local Reynolds numbers ($Re_{\delta_2} \lessapprox 400$) and large values of H_{32} this relation yields $H_{12} < 1$. This behavior, however, should only occur with tangential blowing which is not considered in the present investigations. Therefore an alternative empirical relation[10,13] was derived which ensures $H_{12} > 1$ for any Re_{δ_2} and furthermore satisfies the asymptotic condition $H_{32}(H_{12} \to 1) = 2$ for a rectangular velocity profile.

Reliable transition prediction is of essential importance for successful design and optimization of natural laminar flow airfoils. For the present investigations the semi-empirical e^n-method according to van Ingen[14] and Smith & Gamberoni[15] was implemented. This approach takes advantage of the fact that the transition process in subsonic 2D-flows is typically associated with the growth and breakdown of Tollmien-Schlichting waves (TS-waves). As long as the disturbance amplitude A is small enough, the amplification can be predicted by means of linear stability theory. The basic idea of the e^n-method is that transition may be assumed when the most amplified frequency reaches a certain critical amplification factor $n_{crit.} = \ln\left(A_{crit.}/A_{initial}\right)$. The value of $n_{crit.}$ depends on freestream conditions, the receptivity mechanism and on the definition of the transition 'point'. Therefore, $n_{crit.}$ has to be correlated individually for each wind-tunnel (or for free-flight conditions) taking the numerical model used for the airfoil analysis into account, compare Sec. 4. With the present e^n-implementation, spatial disturbance growth is considered. Since stability analysis based on a direct solution of the Orr-Sommerfeld equation requires too much computational effort for the purpose of numerical airfoil optimization, a database method was implemented. This database contains the amplification rates for 36 shape factors (incl. separated flows) at 40 different Reynolds numbers and 40 different frequencies.

To account for the influence of transitional separation bubbles which are 'short' according to the definition of Tani[16] a new simplified bubble model was developed.[9,10,13] The objective was not to enable a detailed calculation of the flow properties inside the bubble, but

to efficiently determine realistic initial values for the turbulent boundary-layer calculation downstream of the bubble. Thereby, a minimum number of superimposed empirical relations was aspired. Following the classical approach proposed by Horton[17] a constant outer-flow velocity U_e is assumed in the laminar part of the bubble. For this region a new family of boundary-layer profiles has been introduced, which is based on a Falkner-Skan separation profile being successively shifted in wall normal direction. The wall distance of the dividing streamline and, accordingly, the magnitude of δ_1 and H_{12} are assumed to increase linearly with the arc length s, depending on the separation angle γ which is determined by means of an empirical correlation.[9] Downstream of transition, a strong abstraction of the real physics is introduced: The reattachment point is assumed to coincide with the transition point which in turn is connected to an abrupt drop of the outer-flow velocity to the inviscid value. If furthermore $\delta_1 = const.$ and $c_f = 0$ is supposed, the integral momentum equation can be solved analytically in the reattachment region which yields the δ_2-increase over the whole bubble, compare Fig. 11. The main advantage of this approach is that the use of uncertain dissipation laws in the unsteady recirculation region is avoided and a direct, non-iterative calculation is possible.

The drag coefficient of the airfoil is finally determined from the boundary-layer properties at the trailing edge by means of the Squire-Young formula. If turbulent separation is predicted, the inviscid lift coefficient is corrected in a semi-empirical way as proposed by Eppler.[2] In principle, the airfoil design method enables an iterative viscous/inviscid coupling. For the present investigations, however, this option is *not* used in order to minimize the computational effort during the optimization and to reduce the roughness of the objective function considered, see Sec. 5. A more detailed description of the aerodynamic model along with validation examples can be found in other publications of the authors.[9,10]

3 Experimental Set-Up

The experiments were carried out in the Model Wind-Tunnel (MWT)[18,19] of the IAG. The MWT (Fig. 1) is an open return tunnel with a closed test section. It is placed inside a large test hall which ensures stable operation conditions.

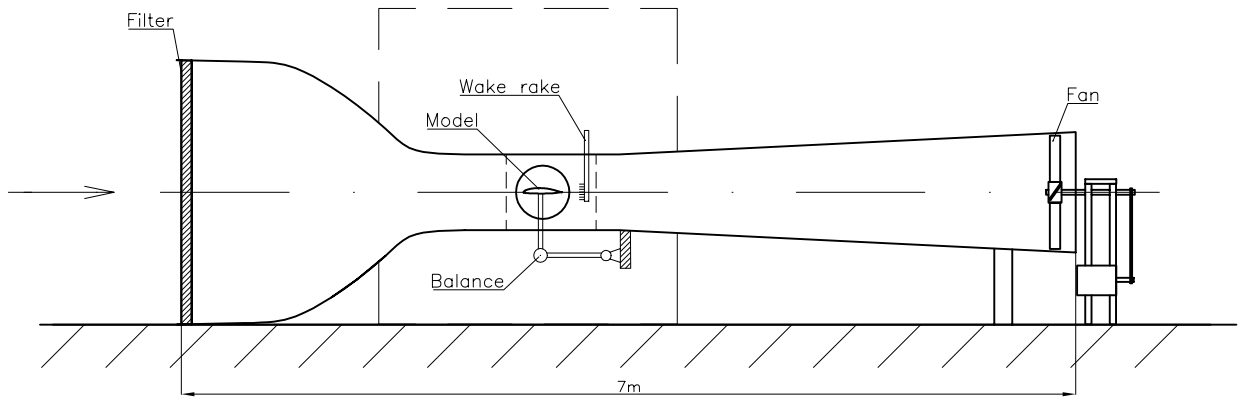

Figure 1: The Model Wind-Tunnel (MWT) of the IAG

The test section measures $0.375 \times 0.6m^2$ and is $0.9m$ long. The 2D airfoil models span the short distance of the test section. A thyristor regulated $4kW$ engine and an adjustable belt drive gives control over the r.p.m. of the 9-bladed fan. Due to the high contraction ratio of 19.6 : 1 the turbulence level (Fig. 2) is between $Tu = 2 \cdot 10^{-4} \sim 8 \cdot 10^{-4}$ depending on the tunnel speed ($4m/s < U_\infty < 30m/s$). Typical chord lengths of the models are in the range of $0.12m \sim 0.2m$ which results in possible Reynolds numbers from $Re = 30,000$ to $Re = 400,000$.

The airfoil models are built of reinforced fiberglass in NC-milled molds to ensure the necessary surface accuracy. A special milling technique is used to reduce the remaining surface roughness of the mold to $0.02mm$. Therefore only a small amount of work is necessary to smooth and polish the surface of the models. The airfoil models are mounted horizontally between two circular end plates which are flush with the tunnel side walls. A special construction of the gap geometry of the end plates reduces leakage effects caused by different static pressure inside and outside the test section. The end plates are connected to a balance with a high precision load cell. The lift is determined directly by this force measurement, whereas the drag is measured indirectly by means of an integrating wake rake.[3,20] The wake rake is positioned 30% of the chord length downstream of the trailing edge and is traversed in spanwise direction to account for drag variations due to longitudinal inherent structures in the boundary layer. Four Furness Controls Ltd. micromanometers are used to measure simultaneously the dynamic head, the mean pressure loss in the wake, the static pressure difference and the maximum pressure loss in the center of the wake. The complete measurement system is highly automated and controlled by a PC equipped with a 12bit A/D converter. Standard wind-tunnel corrections are applied and the results are monitored on-line.

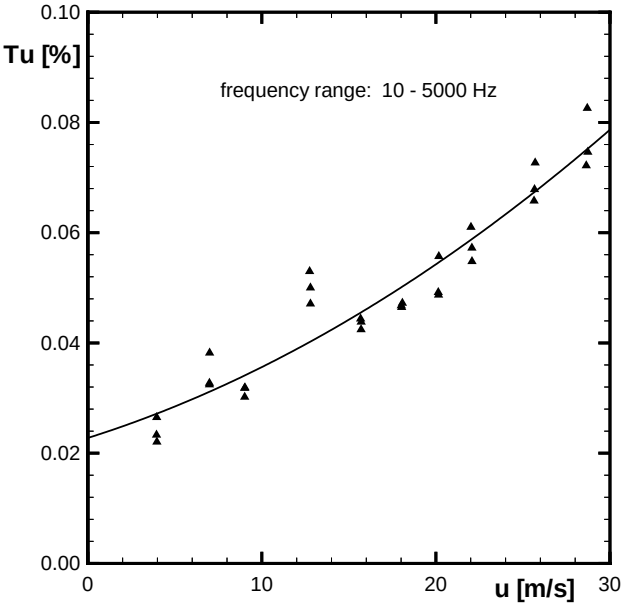

Figure 2: Turbulence level of the Model Wind-Tunnel

4 Correlation of the Critical Amplification Factor for the Model Wind-Tunnel

The application of the e^n-method described in Sec. 2 requires the determination of a limiting n-factor for the test facility (or free flight conditions) in order to enable a realistic recalculation of experiments. Different procedures to determine $n_{crit.}$ are possible. One direct approach is to use the measured turbulence level of the wind tunnel considered together with available correlations for $n_{crit.}$.[21,22] The main disadvantage with this approach is that

the integral value of the turbulence level is used and the spectral distribution of the velocity fluctuations is neglected. Typically the unstable TS waves are connected with a small frequency range in comparison to the whole range used for the evaluation of the turbulence level. The direct measurement of the velocity fluctuations in this critical frequency range is almost impossible, because of its small amplitude (for low turbulence facilities) which is in the order of the electronic noise of the hot-wire equipment. In addition it is important to distinguish between vorticity and pressure fluctuations which can have the same contribution to the measured turbulence level but, due to different receptivity mechanisms[23] the generated initial TS amplitudes in the boundary layer can differ significantly.

To avoid these problems, an indirect 'calibration' is commonly preferred. The predicted transition positions for several test cases are compared to the experimentally determined location and the n-factor is adjusted until a good match is achieved. This procedure also takes small differences in the numerical evaluation of the n-factor into account because the numerical model is directly involved.

A priori it is not clear, if a similar method can be adopted to the low Reynolds number regime. To establish a well defined test case we designed a special symmetrical airfoil which provides transition without a separation bubble at zero angle of attack. Due to the low test Reynolds numbers ($Re = 200,000$ and $Re = 250,000$) this is quite a challenging problem. The advantage of a symmetrical model is that the zero angle of attack can be adjusted very accurately by measuring the static pressure difference between the lower and upper surface near the leading edge. In addition the pressure distribution, more precisely the circulation of the model, is not affected by possible influences from the wind-tunnel boundary layer. The airfoil was designed to achieve an almost constant shape factor of $H_{12} = 3.3$ between $x/c = 0.15$ and $x/c = 0.95$. To avoid disturbances resulting from pressure orifices the pressure distribution was measured with the help of a miniaturized static pressure probe positioned at the boundary-layer edge. The agreement with the calculated inviscid distribution is very good (see Fig. 3). Based on the theoretical distribution a boundary-layer calculation was performed and used as input for the spatial stability analysis. The resulting amplitude development is depicted in Fig. 4.

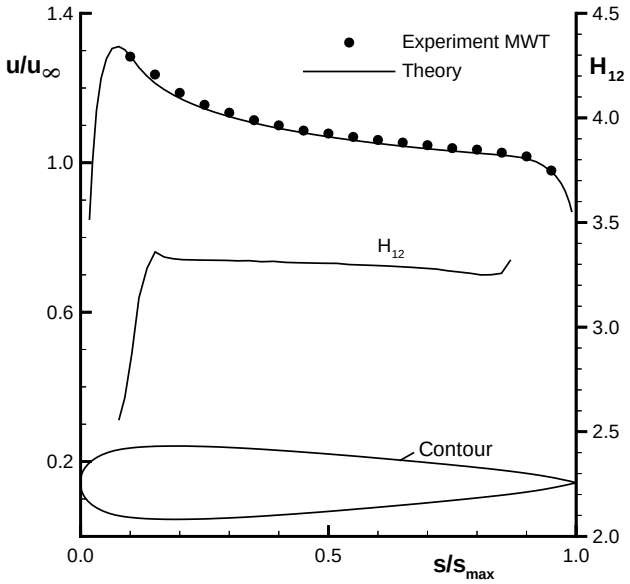

Figure 3: Velocity distribution and development of the shape factor, airfoil GW98-109, $\alpha = 0°$, $Re = 250,000$

The experimental determination of the transition 'point' is a serious problem because transition is a more or less continuous process. Therefore the evaluated position depends strongly on the method used for transition detection. This again has a non-negligible influence on the correlated value of $n_{crit.}$. For the present investigations a classical procedure[24] was applied which is based on the change of the wall shear-stress. A miniature pitot tube

with $0.25mm$ opening is traversed on the surface of the model and the pressure difference to a reference pressure is recorded. Fig. 5 shows the measured data together with a curve fit. For the higher Reynolds number of $Re = 250,000$ the wall shear-stress increases at $s/s_{max} = 0.65$ and reaches its maximum at $s/s_{max} = 0.8$. The corresponding n-factors resulting from Fig. 4 are $n = 12.5$ and $n = 14.5$. The upstream position is similar to the station where first sound can be heard with a stethoscope. The transition 'position' was uniform in spanwise direction.

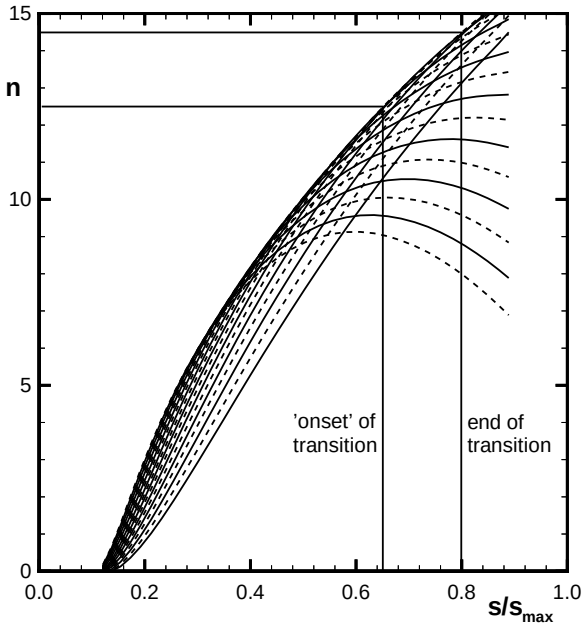

Figure 4: Amplitude development for different TS-frequencies, airfoil GW98-109, $\alpha = 0°$, $Re = 250,000$

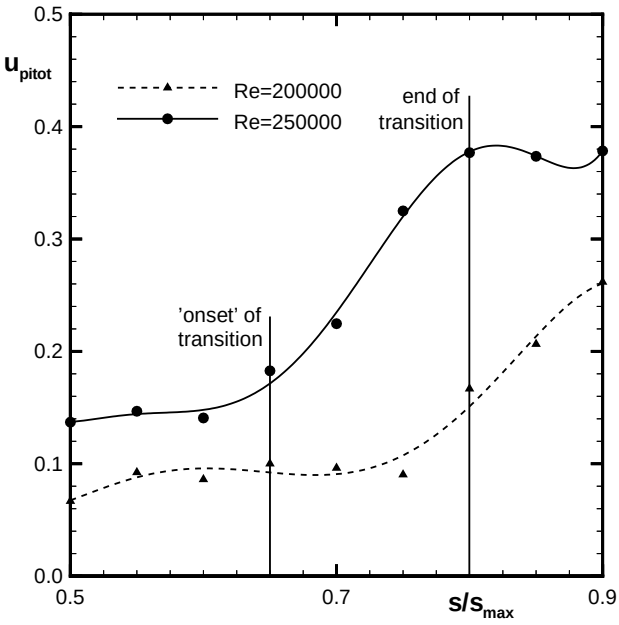

Figure 5: Development of the wall shear-stress in the transition region, airfoil GW98-109, $\alpha = 0°$ (arbitrary scale)

The comparisons for $Re = 200,000$ yields similar n-factors. For the numerical model a rounded value of $n = 12$ is used to predict the location for the switch from laminar to turbulent closure relations. According to the considerations above this position indicates the 'onset' of transition and therefore the first station where the mean velocity profile is influenced by the transition process. It must be noted that basically an inviscid pressure distribution was used for the comparison with the experimental distribution. First of all because the agreement is very good (see Fig. 3) and second to be consistent with the numerical model applied for the present airfoil optimizations (Sec. 5). To check the results, an analogous deduction was performed on the basis of a calculated viscous pressure distribution. The influence of the boundary-layer displacement is very small because of the zero angle of attack, and therefore the evaluated n-factors are only slightly lower ($n = 11.9$ and $n = 13.7$).

5 Numerical Optimization of Low Reynolds-Number Airfoils

Optimization Algorithm

With direct numerical optimization an automated search for an optimal solution with respect to a user-specified objective function, e. g. minimization of the drag coefficient, is performed. This is done by means of an iterative variation of the design variables chosen. For airfoil optimizations it is usually necessary to introduce geometric or aerodynamic constraints like a limitation of the thickness or of the moment coefficient.

Regarding the optimization algorithm deterministic methods, like gradient-based approaches, and stochastic methods, like evolution strategy or genetic algorithm can be distinguished. In general, gradient methods converge fast for a simple topology of the objective function but may get trapped in a local optimum. As a result, the 'optimized' airfoil can look very similar to the initial shape. Actually this is true for most of the numerical airfoil optimizations published so far. Stochastic algorithms offer a greater chance to find a better optimum and furthermore can cope with complex topologies of the objective function. However, usually much more iterations and therefore airfoil analysis are required. Since the objective function considered with the present investigations shows multimodal behavior and strong nonlinearities[10] a hybrid optimizer was applied. The POINTER tool[25] chosen enables constrained optimization and consists of a combination of genetic algorithm, downhill simplex and gradient method.

Airfoil Parameterization

To perform numerical optimizations proper design variables have to be chosen, i. e. the airfoil has to be parameterized in an adequate way. Typically, geometric shape functions like Legendre polynomials, Wagner functions or bezier splines are applied with the respective coefficients used as design variables. The shape functions may directly define the airfoil contour or represent perturbations of a given basic shape.

For the present investigations another approach was preferred. Instead of optimizing the contour in a direct way, the inverse conformal mapping procedure according to Eppler has been applied to generate the airfoil shape. The input parameters α_i^* of this approach were used as design variables for the optimization process. The α_i^*-values represent the angle of attack (relative to the zero-lift line) for which the outer-flow velocity in a certain section i is intended to be constant. This approach has the advantage that the α_i^*-values directly control the local pressure gradient and finally the boundary-layer characteristics. Furthermore, a spline representation of the sensitive leading-edge region is avoided.

Optimization Examples

The objective of the present investigations was to optimize airfoils with minimized average drag coefficient for a set of given angles of attack relative to the inviscid zero-lift line:

$$\sum c_d \left(\alpha_{design},\, Re_{design}\right) \stackrel{!}{=} Min. \tag{1}$$

$$\alpha_{design} = 0^\circ,\, 1^\circ,\, 2^\circ,\, 3^\circ,\, 4^\circ,\, 5^\circ,\, 6^\circ \quad \text{(rel. to zero-lift line)} \tag{2}$$

From the specified α-regime a design lift range of $0 \lessapprox c_{l_{design}} \lessapprox 0.66$ can be estimated. Prescribing fixed values for α was preferred to a direct specification of $c_{l_{design}}$ in order to avoid an α-iteration or an interpolation of the predicted drag polar.

Altogether, three different Reynolds numbers were considered, namely $Re = 2 \cdot 10^5$, $3 \cdot 10^5$ and $4 \cdot 10^5$. Since an experimental verification in the model wind-tunnel of the institute was planned, a value of $n_{crit.} = 12$ being representative for this facility (compare Sec. 4) was specified for transition prediction.

A first optimization run for $Re_{design_I} = 2 \cdot 10^5$ was performed starting from a redesigned NACA $66_2 - 415$ section as the initial airfoil. No geometric or aerodynamic constraints were introduced at all. Thus, the optimization process was driven solely by the objective to minimize the aerodynamic drag. In order to enable a detailed representation of the airfoil shape, a large number of 34 α_i^*-values were chosen as design variables. During the optimization run up to 300,000 airfoils were generated and analyzed which required almost $100h$ CPU time on a desktop workstation. Further optimizations were performed for $Re_{design_{II}} = 3 \cdot 10^5$ and $Re_{design_{III}} = 4 \cdot 10^5$. The resulting airfoil contours are depicted in Fig. 6. It is obvious that the shapes completely differ from the 15% thick NACA airfoil. As expected, the airfoil thickness reduces with decreasing design Reynolds number. The absolute value of t/c is furthermore determined by the design lift range which is identical for all present optimization examples.

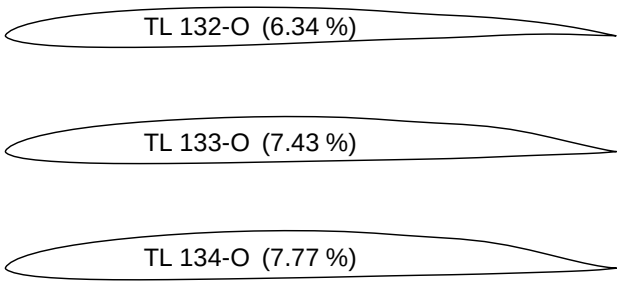

Figure 6: Shapes of the optimized airfoils for $Re_{design} = 2 \cdot 10^5$, $3 \cdot 10^5$ and $4 \cdot 10^5$ (from top to bottom)

The TL 133-O airfoil being optimized for $Re_{design_{II}} = 3 \cdot 10^5$ will now be discussed in more detail. In Fig. 7 the inviscid velocity distributions for different angles of attack (dashed lines) are given. On the lower side the airfoil shows no significant pressure recovery and for $Re_{design_{II}}$ the boundary-layer is predicted to be laminar up to the trailing edge. On the other hand, a steep almost linear flow deceleration was introduced on the suction side. Upstream of the pressure recovery a remarkable valley can be observed in the inviscid velocity distribution. The upstream flank of the valley causes laminar separation and reattachment is predicted to occur at the end of the valley, just upstream of the main pressure recov-

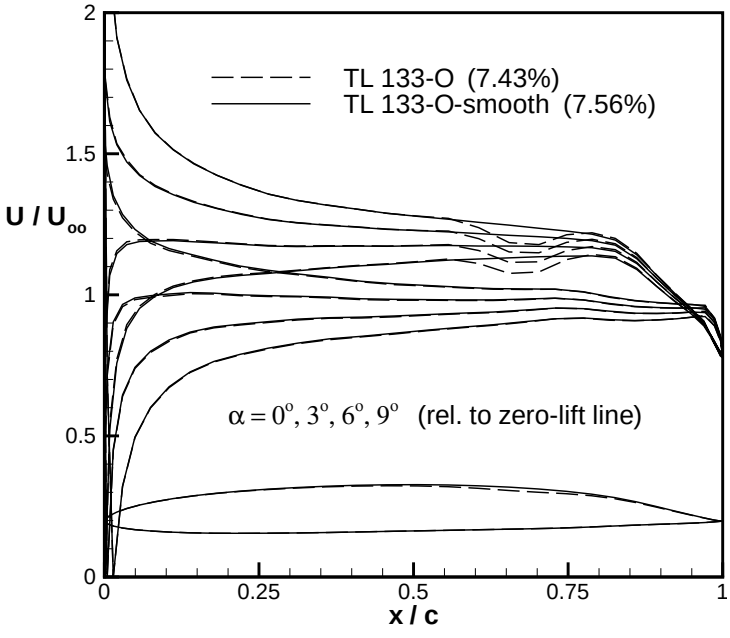

Figure 7: Shapes and inviscid velocity distributions of the original and the modified TL 133-O airfoil

ery. By these means transition is fixed to the ideal position. The turbulent boundary layer is then able to overcome the pressure rise without separation up to the trailing edge.

For the specified design conditions obviously transition initiated by a provoked separation bubble is preferred by the optimizer instead of a continuous destabilization of the attached boundary layer. However, this result may be attributed to the limited design range or to the simplified bubble model applied, which determines the δ_2-increase over the bubble only from *local* flow properties at the separation and reattachment point respectively (compare Sec. 2). Therefore, with the present aerodynamic model the velocity distribution inside of the bubble does not affect the predicted drag directly.

It was decided to examine the physical characteristics of such a special valley-shaped velocity distribution in future experimental studies. For the present investigation we preferred to locally smooth the optimized velocity distribution and to apply an artificial turbulator upstream of the main pressure recovery. The corresponding airfoil shape was calculated by means of a mixed-inverse method, see Fig. 7.

Experimental Verification and Discussion

The locally modified shape was tested in the MWT with a bump tape turbulator ('Noppenband') on the suction side at 77% chord length. A comparison of the measured drag polar and the theoretical result assuming forced transition at the turbulator position is given in Fig. 8. The measurement is reproduced quite reasonably by the present aerodynamic model. The drag polar shows a distinct laminar bucket which coincides with the design lift region. At first view the optimization seems to be successful with respect to the objective function considered. To further examine the quality of the airfoil comparative wind-tunnel tests were

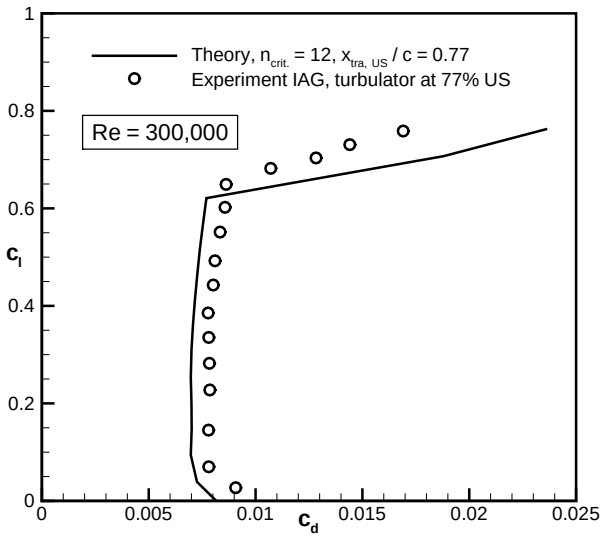

Figure 8: Drag polars for the optimized airfoil TL 133-O-smooth, experiment MWT, $Re = 3 \cdot 10^5$

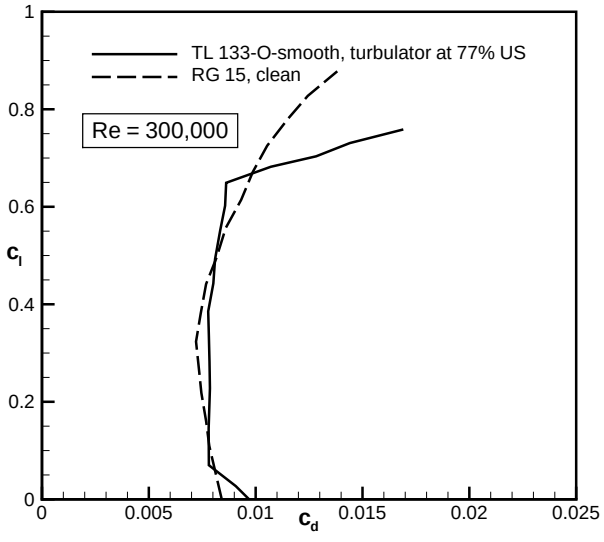

Figure 9: Comparison of the measured drag polars for the optimized airfoil TL 133-O-smooth and the RG 15 section, experiment MWT, $Re = 3 \cdot 10^5$

performed for a manually designed airfoil, namely the RG-15 section (Fig. 10). This airfoil

has proven very successful in model glider applications but was *not* especially designed for the design conditions considered with the present optimization. Therefore, it should be expected that it is inferior at least in the design lift region according to Eq. (2). However, the comparison of the measured drag polars as depicted in Fig. 9 shows that the average drag coefficient in this region is almost identical for both airfoils ($\overline{c_d} = 0.008$ for the RG-15 and $\overline{c_d} = 0.0081$ for the TL 133-O-smooth). The RG-15 offers a lower minimum drag coefficient whereas the optimized airfoil has some gain near the upper edge of the laminar bucket.

This result, in fact, is somewhat disappointing. The reason for the moderate performance of the present optimization result may first of all be attributed to weak points of the aerodynamic model applied for the optimization. Furthermore, the modification of the optimized shape may have a negative impact on the drag characteristics which has to be verified by supplementary wind-tunnel tests. Actually, the modification causes an increase of the *predicted* minimum drag level compared to the original TL 133-O.

A further examination of the RG-15 shows that long but shallow separation bubbles occur on both airfoil sides in the minimum drag region. Whereas on the suction side transition is observed at $x_{tra}/c \approx 0.85$, the boundary layer remains laminar up to the trailing edge on the pressure side. As discussed in the last section this approach seems to be advantageous compared to a design with distinct transition and a subsequent steep pressure recovery. This problem was discussed for example by Pfenninger[6] who preferred a distinct concave main pressure recovery in combination with transition control by means of a suitable turbulator. To investigate this problem on a theoretical basis it is necessary to account for viscous/inviscid interaction effects. Furthermore, the application of the Squire-Young formula to determine the drag is questionable in case of separation bubbles which extend almost into the wake. Direct numerical optimizations considering these problems (e. g. by using the XFOIL-code), maybe for a reduced number of design variables, would therefore be valuable to obtain more insight into the problem of optimum shape design for low Reynolds-number airfoils.

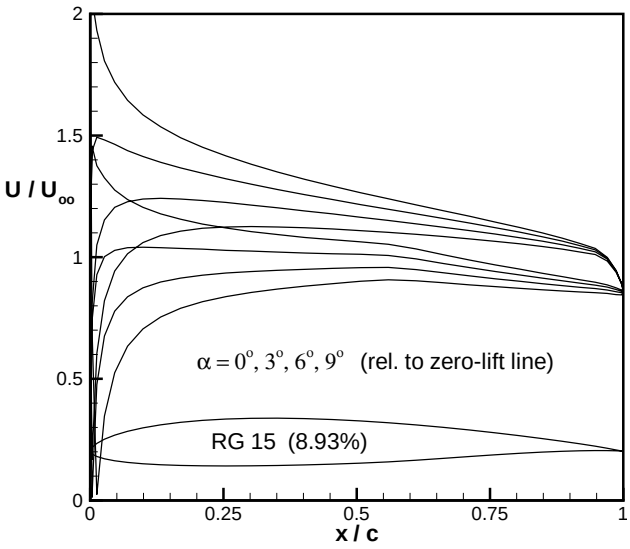

Figure 10: Shape and inviscid velocity distributions of the RG-15 airfoil

6 Experimental Investigations on Very Low Reynolds-Number Airfoils

At Reynolds numbers above $Re = 1 \cdot 10^6$ the design of the airfoil leading-edge is an important task because of the fundamental influence on the width of the low drag bucket and the stall behavior.[26] If the leading edge is too 'sharp', then a pronounced suction peak occurs directly

at the leading edge for angles of attack slightly above the laminar bucket. This suction peak will cause an almost rapid jump of the transition position towards the leading edge which in turn produces a fast forward movement of the turbulent boundary-layer separation. The stall characteristics of such an airfoil design are poor, i. e. an abrupt breakdown in lift has to be expected. On the other hand, if the nose is too blunt, over-velocities are induced downstream of the leading edge and the transition position moves upstream for lower angles of attack than with an ideal nose geometry. This reduces the width of the low drag bucket. However, the stall behavior will be more gentle compared to an airfoil with small nose radius. In any case, at higher Reynolds numbers a laminar separation bubble near the leading edge should be prevented because of possible bubble 'bursting'[27] which will cause a sudden stall.

At low Reynolds numbers the situation is somewhat different. First of all the influence of laminar separation bubbles is much more pronounced. Second, the stability characteristics of the laminar boundary layer are more favorable, therefore it is much easier to achieve a long laminar run. For Reynolds numbers below $Re \approx 100,000$ the problem arises how to obtain a turbulent boundary layer prior to an extended laminar separation which will cause significant additional drag. The common way to solve this problem is the application of an artificial turbulator on the suction side. In general, the lower surface is designed to be fully laminar. A fixed turbulator on the upper surface has one main disadvantage: if it has to be effective at higher lift coefficients then the turbulator has to be placed far upstream. So, if a multi-point design is considered, at lower values of c_l the turbulator will force earlier transition than achievable with a clean airfoil.

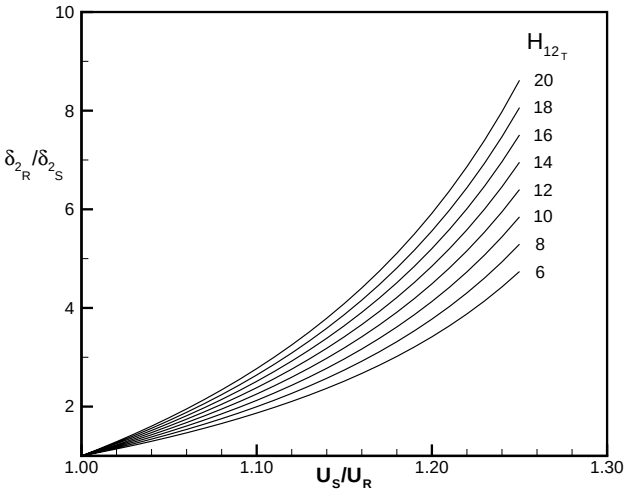

Figure 11: Relative δ_2-increase over a transitional separation bubble in dependence of the maximum shape factor H_{12_T} and the outer-flow velocity ratio U_S/U_R according to the present bubble model

A possible approach to avoid this disadvantage may be the controlled use of a transitional separation bubble near the leading edge. The bubble can be forced to occur at higher angles of attack by a steep pressure rise resulting from a 'sharp' leading edge. For lower angles of attack the suction peak is not present and a longer laminar run results. A leading-edge bubble must not increase the drag significantly if no premature turbulent separation is caused. This can be seen in Fig. 11 where the relative δ_2-increase over a transitional separation bubble is depicted as it results from the simplified bubble model described in Sec. 2. The growth of δ_2 which finally determines the drag increase is proportional to the momentum thickness δ_{2_S} at the laminar separation point S which is small near the leading edge.

Three airfoils were designed to investigate the effect of such a forced leading-edge bubble. Because of the low design Reynolds number of $Re = 50,000$ it was preferred to examine the influence of systematic geometric modifications of a known airfoil rather than to design a completely new shape using theoretical methods. To reduce the number of parameters to be varied, a symmetrical airfoil (NACA 0009) was chosen as initial shape.

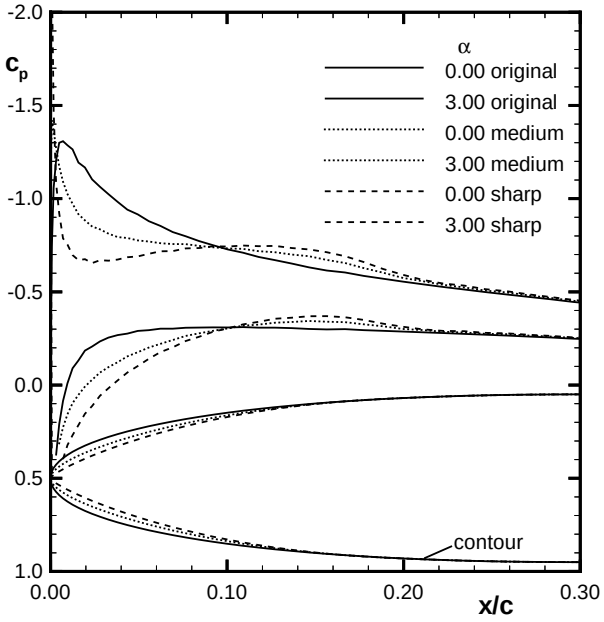

Figure 12: Inviscid pressure distributions of the NACA 0009 and modifications

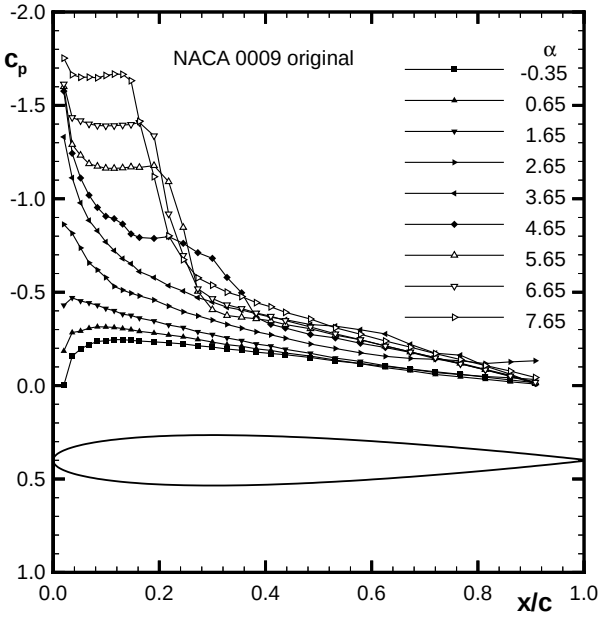

Figure 13: Measured pressure distributions NACA 0009, suction side, experiment MWT, $Re = 50,000$

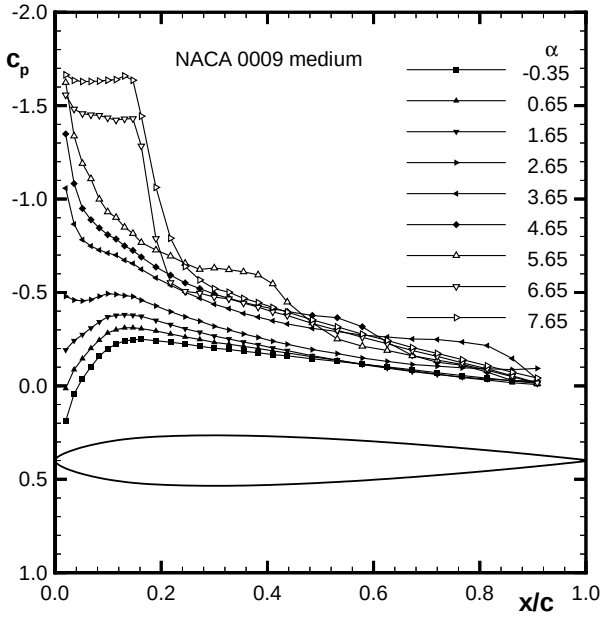

Figure 14: Measured pressure distributions NACA-0009 'medium', suction side, experiment MWT, $Re = 50,000$

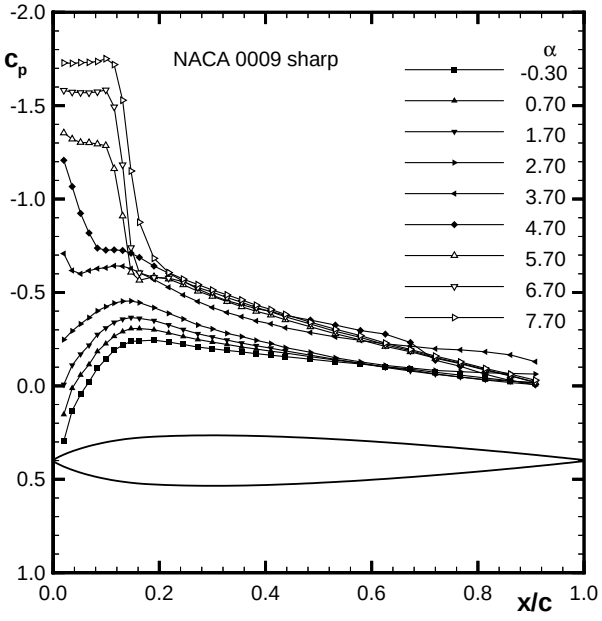

Figure 15: Measured pressure distributions NACA-0009 'sharp', suction side, experiment MWT, $Re = 50,000$

With the present study the influence of the leading-edge radius r_{le} was investigated. Two mutations of the NACA 0009 ($r_{le}/c = 0.0089$) were generated by specifying a reduced value for r_{le} but retaining the original contour for $x/c \geqq 0.1654$. The coordinates in-between

were obtained from a polynomial approximation spline which ensures a smooth curvature distribution near the junction. The resulting airfoils show nose radii of $r_{le}/c = 0.00074$ (designated 'sharp') and $r_{le}/c = 0.0036$ (designated 'medium'), respectively. In Fig. 12 the shapes and the inviscid pressure distributions for the airfoils examined are presented. The modified airfoil sections exhibit a small over-velocity near the junction and also the desired suction peak near the leading edge.

The wind-tunnel models were built with 30 pressure orifices on one side of the airfoil in order to measure the pressure distribution. A special NC-milled template was used to drill the holes with a diameter of $d = 0.3mm$ exactly perpendicular to the surface. The pressure orifices were connected to a scanivalve system and a micromanometer. The pressures were measured according to $c_p = 1 - q/q_\infty$. An integration time of 3 seconds was sufficient to obtain a reliable mean value. No wind-tunnel corrections were applied to the data. Figs. 13 – 15 show the measured distributions for different angles of attack. Due to a small offset in the α-calibration the distributions were not measured at the same angles of attack.

For $\alpha < 3^\circ$ the distributions show the same characteristics as the inviscid calculations, despite the fact that there is a laminar flow separation without reattachment in the rear part. The transition position was checked with a stethoscope. With increasing angle of attack the laminar separation moves upstream and forms a closed separation bubble. This forward movement starts *earlier* for the original NACA-0009 and the 'medium' contour. For $\alpha > 6^\circ$ the separation bubble begins just after the leading edge. As expected, the total length of the bubble is shortest for the sharp leading edge. However, due to the high over-velocity at the separation point, a higher pressure recovery is observed in the reattachment region. This increases the momentum thickness. It can also be seen, that the gradient of the pressure recovery has become steeper for the modified leading edges. The measured distributions for $\alpha \approx 5^\circ$ show no clear picture for all cases examined. From the general behavior it looks as if an unsteady separation bubble exists between $x/c = 0.2 \sim 0.4$. This was checked for the original airfoil with the stethoscope. If the stethoscope was placed at $x/c = 0.3$ and at the boundary-layer edge a 'flapping' can be heard which indicates a rapid upstream/downstream movement of the transition position. Due to the small diameter of the pressure orifices and the necessary tube length unsteady effects can not be resolved and the c_p-distribution shows mean values.

Fig. 16 shows the lift coefficient plotted versus angle of attack. As a result of the laminar separation without reattachment (subcritical state) at angles of attack below 3° the gradient of the lift curve is much lower than the theoretical inviscid lift slope ($dc_l/d\alpha = 2\pi$ for a flat plate). Above 3° the turbulent reattachment process started, i. e. a separation bubble is formed which moves upstream with increasing angle of attack. A steep c_l-increase results for this α-regime. For $\alpha > 5^\circ$ the lift slope again is clearly below 2π which may be caused by the turbulent boundary-layer displacement effect. The $c_{l_{max}}$ is highest for the airfoils with the modified leading edge. The stall behavior is moderate for all configurations.

Fig. 17 shows the measured drag characteristics. Despite of the strong modifications in the leading edge region the drag polars are quite similar. The subcritical range of $-0.2 < c_l < 0.2$ shows no increase in drag due to separation effects. A small advantage of the 'medium' airfoil can be observed for $c_l \approx 0.5$.

The measurements show that the intended behavior could not be achieved for the Reynolds number considered with the variation of only one parameter, namely the leading-edge radius.

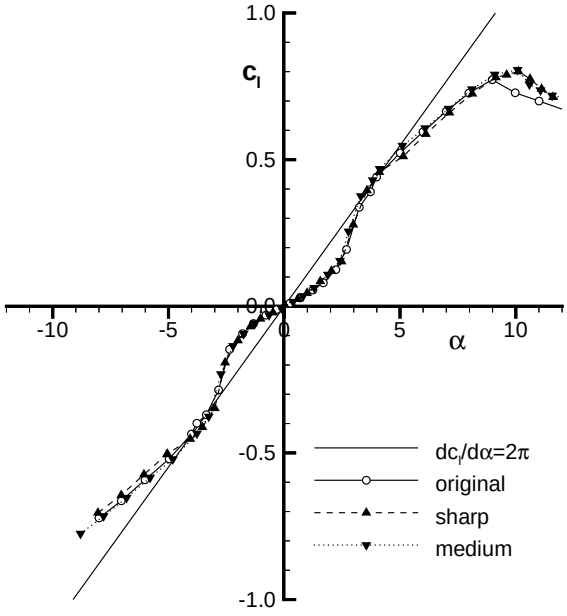

Figure 16: Measured lift coefficients vs. angle of attack, NACA 0009 and modifications, experiment MWT, $Re = 50,000$

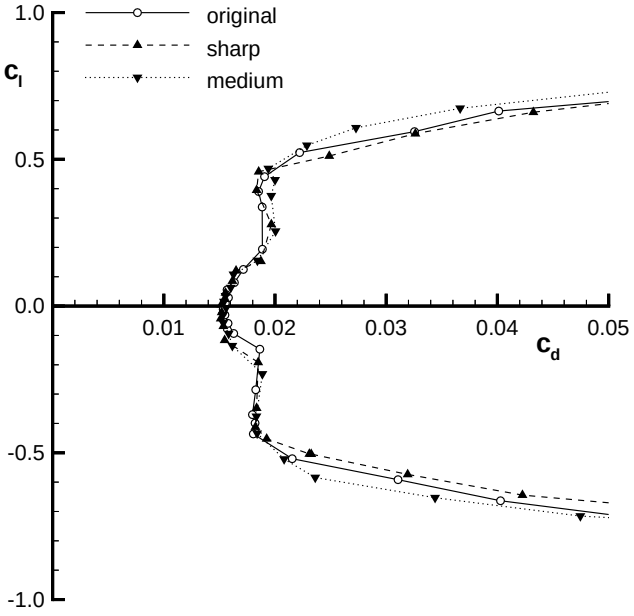

Figure 17: Measured drag polars, NACA 0009 and modifications, experiment MWT, $Re = 50,000$

The main problem is that significant modifications of the inviscid pressure distribution can be egalized due to the dominating viscous effects at such low Re. More combined theoretical and experimental investigations are necessary in future to establish a straight forward design methology for very low Reynolds number airfoils.

7 Conclusion and Outlook

A numerical optimization tool was applied to the design of low Reynolds number airfoils with minimized drag for a specified lift region. The airfoil optimized for $Re_{design} = 300,000$ was tested in the Model Wind-Tunnel of the institute. The predicted drag characteristics is in good agreement to the measured polar and the resulting laminar bucket coincides with the design lift region. The comparison to a classical manual design (RG-15), however, shows similar integral drag values for the design lift range considered. An improvement could not be achieved with the present optimization which may be attributed to difficulties to model exactly the influence of transitional separation bubbles extending into the wake.

In order to deduce guidelines for the design of very low Reynolds-number airfoils, wind-tunnel tests have been performed at $Re = 50,000$. Thereby, the influence of relevant geometric parameters was investigated. In a first campaign the NACA 0009 plus two modifications showing smaller leading-edge radii were examined. The measurements show that strong viscous/inviscid interaction effects occur along with unsteady flow phenomena resulting from large laminar separation bubbles. To get more insight into the very complex flow physics, the leading-edge separation phenomena will be further studied applying different flow visualization techniques. A careful interpretation and a comparison of measurement and theoretical

prediction will be necessary to finally establish proper airfoil design criteria for this special Reynolds-number regime.

References

[1] Drela, M., "Xfoil: An Analysis and Design System for Low Reynolds Number Airfoils," *Low Reynolds Number Aerodynamics (Conference Proceedings)*, edited by T. J. Mueller, University of Notre Dame, 1989.

[2] Eppler, R., "Airfoil Design and Data," Springer Verlag, Berlin/Heidelberg/New York, 1990. ISBN 3-540-52505-X.

[3] Althaus, D., "Niedriggeschwindigkeitsprofile," Friedrich Vieweg & Sohn Verlagsgesellschaft mbH, Braunschweig/Wiesbaden, 1996. ISBN 3-528-03820-9.

[4] Boermans, L. M. M. and van Garrel, A., "Design and Windtunnel Test Results of a Flapped Laminar Flow Airfoil for High–Performance Sailplane Applications," *Technical Soaring*, Vol. 21, No. 1, 1997, pp. 11–17.

[5] Drela, M., "Low–Reynolds–Number Airfoil Design for the M.I.T. Daedalus Prototype: A Case Study," *Journal of Aircraft*, Vol. 25, No. 8, 1988.

[6] Pfenninger, W., and Vemuru, C. S., "Design of Low Reynolds Number Airfoils – I," *Journal of Aircraft*, Vol. 27, No. 3, March 1990.

[7] Selig, M. S., Donovan, J. F., and Fraser, D. B., "Airfoils at Low Speeds," Soartech No. 8, H. A. Stokeley, 1504 North Horseshoe Circle, Virginia Beach, Virginia 23451, USA, 1989.

[8] Selig, M. S. et al., "Summary of Low–Speed Airfoil Data Volume 1 – 3," Department of Aeronautical and Astronautial Engineering, University of Illinois at Urbana–Champaign, 1995, 1996, 1998.

[9] Lutz, Th., "Berechnung und Optimierung subsonisch umströmter Profile und Rotationskörper," Dissertation, Institut für Aerodynamik und Gasdynamik, Universität Stuttgart, 2000. VDI Fortschritt–Berichte, Reihe 7: Strömungstechnik, Nr. 378, ISBN 3-18-337807-8.

[10] Lutz, Th., and Wagner, S., "Numerical Shape Optimization of Subsonic Airfoil Sections," In *ECCOMAS 2000: European Congress on Computational Methods in Applied Sciences and Engineering, September 11–14, 2000, Barcelona, Spain*, 2000. To be published.

[11] Schmitz, F. W., "Aerodynamik des Flugmodells," Luftfahrt und Schule/Reihe IV/Band 1, C. J. E. Volckmann Nachf. E. Wette, Berlin-Charlottenburg 2, 1942.

[12] Hamma, W., "Neu entwickelte Tragflügelprofile für $Re < 10^5$ mit den zugehörigen Polaren und Ergebnissen aus Grenzschichtbeobachtungen an diesen Profilen," Diploma thesis (Teil II), Institut für Aerodynamik und Gasdynamik, Technische Hochschule Stuttgart, 1963.

[13] Weigold, W., "Untersuchungen zur halbempirischen Ermittlung des Umschlags in laminaren Ablöseblasen und Programmierung eines vereinfachten Blasenmodells," Diploma thesis, Institut für Aerodynamik und Gasdynamik, Universität Stuttgart, 1998.

[14] van Ingen, J. L., "A Suggested Semi–Eempirical Method for the Calculation of the Boundary Layer Transition Region," Report V.T.H. 71, V.T.H. 74, Department of Aeronautical Engineering, Delft University of Technology, 1956.

[15] Smith, A. M. O., and Gamberoni, N., "Transition, Pressure Gradient and Stability Theory," Report ES 26388, Douglas Aircraft Company, 1956.

[16] Tani, I., "Low–Speed Flows Involving Bubble Separations," *Progress in Aeronautical Sciences*, Vol. 5, pp. 70–103, Pergamon Press, New York, 1964.

[17] Horton, H. P., "A Semi–Empirical Theory for the Growth and Bursting of Laminar Separation Bubbles," Current Paper (C.P.) No. 1073, Ministry of Technology, Aeronautical Research Council, Queen Mary College, University of London, 1969.

[18] Althaus, D., "Profilpolaren für den Modellflug I," Neckar Verlag, Villingen–Schwenningen, 1980.

[19] Althaus, D., "Profilpolaren für den Modellflug II," Neckar Verlag, Villingen–Schwenningen, 1985.

[20] Abbott, I. H., von Doenhoff, A. E., and Stivers, L. S., "Summary of Airfoil Data," NACA Rept. 824, NACA, 1945.

[21] Mack, L. M., "A Numerical Method for the Prediction of High–Speed Boundary–Layer Transition Using Linear Theory," NASA SP 347, NASA, 1975.

[22] van Ingen, J. L., and Boermans, L. M. M., "Research on Laminar Separation Bubbles at Delft University of Technology in Relation to Low Reynolds Number Airfoil Aerodynamics," *Proceedings Conference on Low Reynolds Number Airfoil Aerodynamics, UNDAS-CP-77B123*, pp. 89–124, University of Notre Dame, Indiana, USA, 1985.

[23] Saric, W. S., "Laminar–Turbulent–Transition: Fundamentals," *AGARD Report 786: Special Course on Skin Friction Drag Reduction*. AGARD, 1992.

[24] Schubauer, G. B., and Skramstad, H. K., "Laminar Boundary Layer Oscillation and Transition on a Flat Plate," NACA Rept. 909, NACA, 1948.

[25] Synaps Inc., *Pointer Optimization Software Release 1.1 User's Guide*, 2957 Clairmont Road, Suite 170, Atlanta, GA 30329, USA, 1997.

[26] Althaus, D., "Effects on the Polar due to Changes or Disturbances to the Contour of the Wing Profile," *Technical Soaring*, Vol. 10, No. 1, 1986.

[27] Gaster, M., "The Structure and Behaviour of Laminar Separation Bubbles," *AGARD CP-4 'Flow Separation Part II'*, pp. 813–854, NATO AGARD, 1966.